

RESEARCH ARTICLE | MARCH 07 2023

# On the resilience of dual-waveguide parametric amplifiers to pump power and phase fluctuations

M. Shi ; V. Ribeiro ; A. M. Perego  

 Check for updates

*Appl. Phys. Lett.* 122, 101102 (2023)

<https://doi.org/10.1063/5.0136729>

  
View  
Online

  
Export  
Citation

CrossMark

## Articles You May Be Interested In

Resiliency of gymnasium floors

*J Acoust Soc Am* (August 2005)

On quaternary resilient functions

*AIP Conference Proceedings* (July 2023)

Evolution and resilience of the nuclear nonproliferation regime

*AIP Conference Proceedings* (May 2014)

### 500 kHz or 8.5 GHz? And all the ranges in between.

Lock-in Amplifiers for your periodic signal measurements



Find out more



# On the resilience of dual-waveguide parametric amplifiers to pump power and phase fluctuations

Cite as: Appl. Phys. Lett. **122**, 101102 (2023); doi: [10.1063/5.0136729](https://doi.org/10.1063/5.0136729)

Submitted: 28 November 2022 · Accepted: 14 February 2023 ·

Published Online: 7 March 2023



View Online



Export Citation



CrossMark

M. Shi,  V. Ribeiro, <sup>a)</sup>  and A. M. Perego <sup>b)</sup> 

## AFFILIATIONS

Aston Institute of Photonic Technologies, Aston University, Birmingham B4 7ET, United Kingdom

<sup>a)</sup>Present address: KETS Quantum Security Ltd., Station Road Workshops, Bristol BS15 4PJ, United Kingdom.

<sup>b)</sup>Author to whom correspondence should be addressed: [a.perego1@aston.ac.uk](mailto:a.perego1@aston.ac.uk)

## ABSTRACT

Parametric amplifiers based on coupled-core fibers and coupled integrated waveguides are promising devices for delivering broadband and flat gain spectrum with low noise figure in vital technological applications such as optical communications. To address potential practical issues that may arise in the experimental demonstration, in the present work, we derive analytical expressions for the impact of relative input pump phase and power fluctuations between two waveguides on pump waves stability. We, furthermore, evaluate, through numerical simulations, how the pump power oscillations between the two waveguides affect the amplifier spectrum, identifying optimal regimes of operation for coupled-core fibers and also for coupled integrated waveguides. Our findings hint at the resilience of these parametric amplifiers' architectures and at their possible practical implementation in realistic labs and real-world scenarios.

© 2023 Author(s). All article content, except where otherwise noted, is licensed under a Creative Commons Attribution (CC BY) license (<http://creativecommons.org/licenses/by/4.0/>). <https://doi.org/10.1063/5.0136729>

Optical parametric amplifiers relying on four-wave mixing enabled by Kerr nonlinearity<sup>1–3</sup> are a promising technology offering broadband amplifications for optical communications<sup>4–8</sup> and which also find applications for frequency conversion.<sup>9</sup> Parametric amplifiers have been traditionally demonstrated using silica fibers and also in integrated silicon<sup>10</sup> and silicon nitride waveguides.<sup>11–15</sup> Alternative architectures based on coupled-core fibers and coupled waveguides are possible as well. Parametric amplification in two coupled nonlinear waveguides was originally proposed in seminal contributions a few decades ago.<sup>16–18</sup> The related study of modulation instability has been afterward theoretically addressed by other authors for asymmetric continuous waves solutions,<sup>19</sup> including higher-order effects,<sup>20</sup> with gain in one of the waveguides,<sup>21</sup> including the frequency dependency of the coupling<sup>22</sup> (also with polarization effects,<sup>23</sup> higher-order dispersion,<sup>24,25</sup> and saturable nonlinearity<sup>26</sup>) with asymmetry between the coupled cores,<sup>27</sup> and also in fibers with a larger number of coupled cores.<sup>28,29</sup> However, only recently, research attempts to bring coupled-waveguide parametric amplifiers closer to technology have been performed, including theoretical studies<sup>30–33</sup> and preliminary experimental demonstrations.<sup>34,35</sup> The potential benefits of parametric amplifiers based on the two coupled waveguides architecture lie in the flatness of the gain spectrum,<sup>30</sup> together with the low noise figure in a phase-sensitive mode.<sup>31</sup> This geometry provides extra degrees of freedom, which enable compensation of phase-matching degradation due to

pump attenuation in lossy integrated waveguides exploiting spatial engineering of the coupling,<sup>32,34</sup> dispersion compensation,<sup>36</sup> and parametric amplification with signal and idler separation between different supermodes<sup>37</sup> harnessing the frequency dependency of the coupling strength. Several impairments could affect the performance of coupled-waveguide parametric amplifiers pumped with two equally powerful pump waves. These include: relative power and phase differences between the pump waves in the two waveguides, random fluctuations of the zero-dispersion wavelength and their correlation between the two waveguides, and parameters difference among the two waveguides—such as group velocity dispersion and nonlinearity—arising during the fabrication process. In this work, we analytically and numerically study the first one of these potential impairments, namely, the impact of pump power and phase fluctuations between the two coupled waveguides on the amplifier performances for an amplifier operating in the regime where the two waveguides are pumped with equal power. We have derived an analytical formula, which describes the spatial instability—leading to power exchange and oscillations of the continuous waves solutions between the two coupled waveguides during propagation—resulting from the small and unwanted time-independent perturbations caused by the relative differences in input power and phase. We show that the predictions of the analytical formula agree well with numerical solutions of the pump wave propagation along the waveguides. We, furthermore, numerically investigate

the impact of the input pump phase and power difference on the amplifier gain for parameters typical of coupled-core silica fibers and also for integrated silicon nitride waveguides, showing that the amplifier is robust against the fluctuation magnitude within the possibility of realistic experimental control. The starting point of our theory consists of two nonlinear Schrödinger equations (NLSEs), which rule the propagation of the electric field amplitudes  $A_{1,2}$  along two identical coupled waveguides

$$\frac{\partial A_1}{\partial z} = i \sum_{n=0}^{\infty} \frac{\beta_n}{n!} (i\partial_t)^n A_1 + i\gamma|A_1|^2 A_1 - \frac{\alpha}{2} A_1 + i \sum_{n=0}^{\infty} \frac{C_n}{n!} (i\partial_t)^n A_2, \tag{1a}$$

$$\frac{\partial A_2}{\partial z} = i \sum_{n=0}^{\infty} \frac{\beta_n}{n!} (i\partial_t)^n A_2 + i\gamma|A_2|^2 A_2 - \frac{\alpha}{2} A_2 + i \sum_{n=0}^{\infty} \frac{C_n}{n!} (i\partial_t)^n A_1. \tag{1b}$$

Here,  $\beta_n$  and  $C_n$  are the  $n$ th coefficient of the Taylor expansion of the frequency-dependent propagation constant  $\beta(\omega)$  and coupling  $C(\omega)$ , respectively,  $\gamma$  and  $\alpha$  are the nonlinearity and attenuation coefficients, respectively,  $t$  is the temporal coordinate, and  $z$  is the spatial evolution coordinate along the longitudinal waveguides dimension. A sketch of a dual-waveguide parametric amplifier is shown in Fig. 1. We consider pumps with amplitudes denoted by  $\bar{u}_{p1,p2}$  to be continuous wave (time-independent) solutions of Eqs. (1). The solutions with the same power  $P_p/2$  and constant phase difference 0 (symmetric) or  $\pi$  (antisymmetric) read

$$\bar{u}_{p1,p2} = \sqrt{\frac{P_p}{2}} e^{-\frac{\alpha}{2}z} e^{i(\phi_p \pm \xi z)}, \tag{2a}$$

$$\phi_p = \phi_0 + [\beta_0 + (-1)^\xi C_0]z + \frac{\gamma}{2} P_p z_{\text{eff}}, \tag{2b}$$

where  $\xi$  is 0 or 1 for symmetric or antisymmetric solution, respectively,  $\phi_0 \pm \xi\pi/2$  are the initial phases of the two pump waves, and  $z_{\text{eff}} = \int_0^z e^{-\alpha z'} dz'$  (in the absence of losses  $z_{\text{eff}} \rightarrow z$ ). To study the stability of the pump waves shown in Eqs. (2), we add small perturbations  $\eta_{1,2}$  ( $|\eta_{1,2}|^2 \ll P_p$ ) at the pump frequency to the solutions  $\bar{u}_{p1,p2}$ , which leads to the following *ansatz*:

$$u_{p1,p2}(z) = \bar{u}_{p1,p2} + \eta_{1,2}(z) e^{-\frac{\alpha}{2}z} e^{i(\phi_p \pm \xi z)}. \tag{3}$$

By redefining  $P_p$  as the total power and selecting a proper  $\phi_0$ , the initial amplitudes in two waveguides can always be written as

$$u_{p1,p2}(0) = \sqrt{\frac{P_p \pm P_d}{2}} e^{i(\phi_0 \pm i\frac{\phi_d \pm \xi z}{2})}, \tag{4}$$

where  $P_d$  and  $\phi_d$  are the initial power difference and phase difference, respectively. Considering  $P_d \ll P_p$  and  $\phi_d \ll 1$ , the amplitudes can be rewritten as

$$\begin{aligned} u_{p1,p2}(0) &\approx \left( \sqrt{\frac{P_p \pm P_d}{2}} \right) \left( 1 \pm \frac{\phi_d}{2} \right) e^{i(\phi_0 \pm \xi z)} \\ &\approx \left( \sqrt{\frac{P_p \pm P_d}{2}} \pm i \frac{1}{2} \sqrt{\frac{P_p}{2}} \phi_d \right) e^{i(\phi_0 \pm \xi z)}, \end{aligned} \tag{5}$$

which implies  $\eta_1(0) = -\eta_2(0) = \frac{P_d}{2\sqrt{2P_p}} + i\frac{1}{2}\sqrt{\frac{P_p}{2}}\phi_d$ . By substituting Eq. (3) into the coupled NLSEs, Eqs. (1), and explicitly writing  $\eta_{\pm} = a_{\pm} + ib_{\pm}$ , where  $\eta_{\pm} = \eta_1 \pm \eta_2$ , we obtain the equations governing the propagation of the perturbations real and imaginary parts as follows:

$$\begin{aligned} \partial_z \begin{pmatrix} a_{\pm} \\ b_{\pm} \end{pmatrix} &= M_{\pm} \begin{pmatrix} a_{\pm} \\ b_{\pm} \end{pmatrix} \\ &= \begin{pmatrix} 0 & \gamma \frac{P_p}{2} e^{-\alpha z} - K_{\pm} \\ \gamma \frac{P_p}{2} e^{-\alpha z} + K_{\pm} & 0 \end{pmatrix} \begin{pmatrix} a_{\pm} \\ b_{\pm} \end{pmatrix}, \end{aligned} \tag{6}$$

where  $K_{\pm} = \gamma \frac{P_p}{2} e^{-\alpha z} + (-1)^\xi (\pm C_0 - C_0)$ . As  $\eta_+(0) \approx 0$  and  $\eta_-(0) \approx \frac{P_d}{\sqrt{2P_p}} + i\sqrt{\frac{P_p}{2}}\phi_d$ , only the evolution of  $\eta_-$  needs to be calculated whereas  $\eta_+$  remains vanishing. An approximate solution to Eq. (6) is  $(a_-, b_-)^T = e^{\int_0^z M_-(z') dz'} (a_-(0), b_-(0))^T$ , where the exponential expression reads

$$N = e^{\int_0^z M_-(z') dz'} = \begin{pmatrix} \cosh \rho & \theta \sinh \rho \\ \theta^{-1} \sinh \rho & \cosh \rho \end{pmatrix}, \tag{7}$$

with  $\rho = \sqrt{-2C_0 z [2C_0 z - (-1)^\xi \gamma P_p z_{\text{eff}}]}$  and  $\theta = (-1)^\xi 2C_0 z / \rho$ . We finally obtain

$$\eta_-(z) = (\cosh \rho + i\theta^{-1} \sinh \rho) \frac{P_d}{\sqrt{2P_p}} + (\theta \sinh \rho + i \cosh \rho) \sqrt{\frac{P_p}{2}} \phi_d. \tag{8}$$

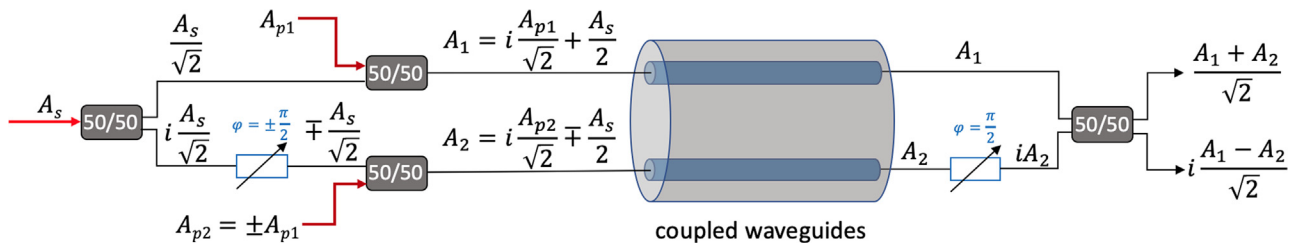


**FIG. 1.** Sketch of a dual-waveguide parametric amplifier.  $A_s$  is the input signal wave, and  $A_{p1,p2}$  are the pump waves in the two waveguides. The components denoted by “50/50” are 50/50% couplers. Blue rectangles with a diagonal arrow describe phase shifters, and one can input even or odd supermodes by switching the phase shifter located before the coupled waveguides between  $\pm \frac{\pi}{2}$ . The second phase shifter and the coupler located after the coupled waveguides enable separation of the amplified supermodes at the output.

To have direct insight into the instability of the symmetric pump power solution, we study the power difference between two waveguides  $P_-(z) = |u_{p1}|^2 - |u_{p2}|^2$ , which can be evaluated as a function of  $\eta_-$  approximately by

$$P_-(z) = e^{-\alpha z} \left( \left| \sqrt{\frac{P_p}{2}} + \frac{\eta_-}{2} \right|^2 - \left| \sqrt{\frac{P_p}{2}} - \frac{\eta_-}{2} \right|^2 \right) = e^{-\alpha z} (P_d \cosh \rho + P_p \phi_d \theta \sinh \rho), \quad (9)$$

where  $\eta_1 = -\eta_2 = \eta_-/2$  is considered. We first focus on the symmetric pump power solution ( $\xi = 0$ ). As the signature flat broadband gain of coupled-waveguide amplifiers is obtained with symmetric pump input when the attenuation is negligible for  $\gamma P_p = 4C_0$ , we will use this relation across the whole paper and as a result  $\theta \approx 1$ . In realistic symmetrically pumped parametric amplifiers,  $\cosh \rho$  is close to  $\sinh \rho$  as the amplifier length  $L$  is larger than the nonlinear length  $L_{NL}$ :  $L > L_{NL} = \frac{1}{\gamma P_p/2}$ . (We consider in this work  $L_{NL} \approx 33$  m for dual-core fibers and  $L_{NL} \approx 28$  cm for integrated waveguides.) Thus, the two expressions enclosed by parentheses in Eq. (8) are approximately equal. As typically the pump power is larger than 1 W, power fluctuations of the order of 1 mW and phase fluctuations of the order of 1 mRad will lead to a similar dynamics of the power imbalance  $P_-$ . Experimentally, it is, in general, more challenging—but still feasible—to control phase differences up to the mRad level rather than it is to control power fluctuations or imbalances up to the mW level, as we will comment more in detail later; hence, we can generally assume that  $\sqrt{\frac{P_p}{2}} \phi_d > \frac{P_d}{\sqrt{2P_p}}$ , and initial phase differences in two waveguides are usually the dominant effect that can induce substantial pump power imbalance upon propagation. In typical optical parametric amplifiers experimental setups, the noise of the pump laser can result in power fluctuations with an optical signal-to-noise ratio (OSNR) between 50 and 70 dB, which for a pump with 1 W average power will put the power or variance of the noise in the sub- $\mu$ W to  $\mu$ W regime. An additional source of power fluctuations is the 3-dB coupler that follows the pump laser (typically composed of a low-power laser source followed by an erbium-doped fiber amplifier). However, as the two optical waves used to pump dual-waveguide parametric amplifiers are, in general, obtained by splitting a powerful wave by means of a 50/50% optical coupler, the main cause of the relative power difference between two pump waves is due to coupler imperfections. The ratio tolerance is within  $\pm 5\%$  in a 100 nm bandwidth for most standard 50/50% couplers, increasing almost monotonically with wavelength shift from their center wavelength. (The ratio tolerance will be in practice much smaller in case the pump is located at the center of the coupler transmission bandwidth.) For a reference value of the pump power on the order of 1 W, this leads to a maximum of  $\pm 50$  mW power imbalance between the pumps, meaning a 100 mW net difference. Note that the physical power difference between the pumps corresponds to  $P_d$  in our notation [see the definition given in Eq. (4)]. Sources of the relative phase difference between the two input pump waves are instead connected to differences in their optical paths—after being split at the 50/50% coupler—which can be due to alignment issues of the fiber components in the setup or to fabrication precision issues in the case of integrated waveguides; for instance, an optical path difference of 1 nm corresponds to approximately 6 mRad phase difference at 1550 nm in

silica. Methods available to substantially reduce the relative input pump power imbalance and to precisely controlling phase differences will be discussed later in the text.

Examples of the pump power difference evolution without losses (using parameters typical of coupled-core fibers) and with losses (using parameters typical of silicon nitride waveguides) are shown in Fig. 2. To study the worst-case scenario, where pump and phase fluctuations contribute to a maximum power difference between the two waveguides, the signs of  $P_d$  and  $\phi_d$  are kept the same in the following analysis. For each case, we considered the impact of various initial pump power differences— $P_d = 0.4, 4,$  and  $40$  mW, the impact of different initial phase differences— $\phi_d = 0.6, 6,$  and  $60$  mRad (corresponding to an optical path difference of  $\sim 0.1, 1,$  and  $10$  nm at wavelength  $\lambda = 1550$  nm in silica), and the combined impact of both initial power and phase differences. For the lossless case [Figs. 2(a)–2(c)], the analytical theory is in excellent agreement with numerical simulation results of the coupled NLSEs up to when most of the power is contained in a single waveguide ( $P_- \approx P_p$ ). The larger the input perturbations, the earlier (along the propagation)  $P_-$  becomes substantial. It is worth mentioning that the simulation results show the power exchange between the two waveguides upon propagation: the power in one waveguide flows into the other one and then goes back at the critical point  $P_- = P_p$ , where all the power is contained in a single waveguide. As the stability analysis is based on the small perturbations assumption, this phenomenon is not captured by the analytical calculations. In the lossy case [Figs. 2(d)–2(f)], we observe that  $P_-$  performs damped oscillations, and agreement between simulations and theory seems quite robust for the parameters considered.

To see how the amplifier gain spectrum is affected by the relative input pump phase and power fluctuations, we performed numerical simulations of Eqs. (1) for parameters corresponding to coupled-core fibers and integrated lossy coupled-waveguide amplifiers, considering terms up to the second order in the waveguide and coupling dispersion. We have simulated amplifiers with characteristics analogous to those used for the perturbation analysis presented in Fig. 2, resulting in the key quantity determining the amplifier gain, namely, the nonlinear phase shift accumulated per waveguide  $\gamma P_p L/2$ , to be up to 4.5 for dual-core fibers and up to 5.4 for integrated waveguides. These values can be considered realistic for parametric amplifiers used in optical communications, where the accumulated nonlinear phase shift ranges approximately between 3 and 5.<sup>6,8,13</sup>

We calculated the phase-insensitive (PI) gain spectrum of supermodes  $A_{\pm} = (A_1 \pm A_2)/\sqrt{2}$  choosing as the initial condition the signals—with frequency larger than the pump ( $\Delta\omega > 0$ )—to be fully located in the supermode  $A_-$  as  $u_{s1}(0) = -u_{s2}(0) = 10^{-4}\sqrt{W}$ , and considering idlers—with frequency smaller than the pump ( $\Delta\omega < 0$ )—to be vanishing,  $u_{i1}(0) = u_{i2}(0) = 0$ . Here,  $u_{s,i,1,2}$  are the sideband waves (subscripts  $s, i$  and 1, 2 denote signal and idler and waveguides 1 and 2, respectively). The gain spectrum of the supermodes  $A_{\pm}$  is, hence, defined as  $G_{\pm}(z) = |u_{s1}(z) \pm u_{s2}(z)|^2 / |u_{s1}(z) - u_{s2}(z)|^2$  and  $G_{\pm}(z) = |u_{i1}(z) \pm u_{i2}(z)|^2 / |u_{i1}(z) - u_{i2}(z)|^2$  for positively and negatively detuned angular frequency  $\Delta\omega$  from the pump, respectively. We first studied how the relative pump power or phase difference alone can impact the amplifier gain spectrum in a similar way: we compared the parametric gain spectrum obtained with ( $P_d = 600$  mW,  $\phi_d = 0$ ) and ( $P_d = 0$ ,  $\phi_d = 100$  mRad). From Eq. (8), we know that  $\eta_-$  would be almost equal in both cases for the chosen value

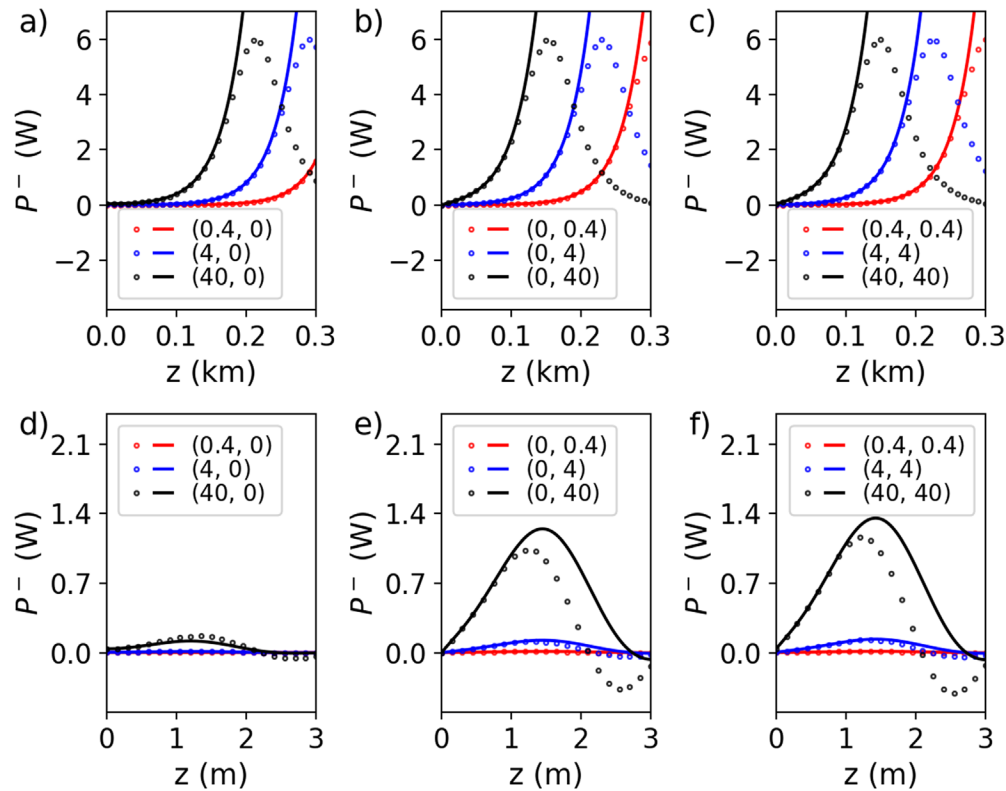


**FIG. 2.** Evolution of pump power difference for the symmetric case.  $P_-$  evolution without losses calculated analytically (solid) and in numerical simulations (dots) for different values of  $P_d$  and  $\phi_d$  shown in the legends, where  $(x, y)$  represents  $P_d = x$  mW and  $\phi_d = y$  mRad. (a)–(c) describe coupled-core fibers and parameters used are  $\gamma = 10 \text{ W}^{-1} \text{ km}^{-1}$ ,  $P_p = 6 \text{ W}$ ,  $C_0 = 15 \text{ km}^{-1}$ , and  $\alpha = 0$ . (d)–(f) Lossy integrated waveguides and parameters used are  $\gamma = 1.2 \text{ W}^{-1} \text{ m}^{-1}$ ,  $P_p = 6 \text{ W}$ ,  $C_0 = 1.8 \text{ m}^{-1}$ , and  $\alpha = 0.69 \text{ m}^{-1}$  corresponding to  $3 \text{ dB m}^{-1}$ .

of the total pump power  $P_p = 6 \text{ W}$ . The results are summarized in Fig. 3 for coupled-core fibers and also for coupled integrated lossy waveguide parameters.

We have then explored the impact on the parametric gain of different magnitudes of pump power and pump phase fluctuations and compared different parametric gain profiles obtained with the unperturbed scenario. The sidebands' gain for the lossless dual-core fiber amplifier is shown in Fig. 4 for supermode  $A_-$  and in Fig. 5 for supermode  $A_+$ . For the lossy integrated waveguide amplifier, the gain is shown in Fig. 6 for supermode  $A_-$  and in Fig. 7 for supermode  $A_+$ . Up to  $P_d = 40 \text{ mW}$  and  $\phi_d = 40 \text{ mRad}$ , we observe that for propagation distance  $z \lesssim 100 \text{ m}$  and  $z \lesssim 1 \text{ m}$ , for coupled-core fibers and integrated waveguides, respectively, the main impact of amplitude and phase perturbations is to slightly reduce the maximum gain without substantially affecting the ideal amplifier performance. However, for larger propagation distances and/or for larger values of input power and phase differences (here, we have considered  $P_d = 200 \text{ mW}$  and  $\phi_d = 200 \text{ mRad}$  to illustrate a more extreme case), substantial modifications of the gain spectrum and coupling of energy from the input supermode  $A_-$  to supermode  $A_+$  occur. This results, as well, in a frequency asymmetric gain spectrum for different supermodes due to the interplay between power asymmetry in the two waveguides and  $C_1$ , the first-order term of the coupling Taylor expansion around the

pump frequency. It can be indeed shown that the combination of coupling dispersion and asymmetric pump power among the two waveguides can lead to intermodal four-wave mixing, resulting in coupling between different supermodes and also frequency asymmetric parametric gain spectrum of individual supermodes.<sup>37</sup> We note that significant changes in the gain spectrum start to occur when most of the pump power is contained in a single waveguide ( $P_- \approx P_p$ ) as shown by the evolution of  $P_-$  plotted in each case considered.

In the antisymmetrically pumped ( $\xi = 1$ ) parametric amplifier, the evolution of the pump power difference is still given in Eq. (9), but  $\rho$  keeps imaginary for any distance, so that the pump power difference  $P_-$  oscillates around zero. This is illustrated in Fig. 8. In the antisymmetric scenario, the same initial conditions for signals and idlers as in the symmetric case have been considered, and a more stable parametric amplification is achieved—without the flat gain profile though—as depicted in Figs. 9 and 10, where we can appreciate that spectral gain degradation occurs for much larger values of the perturbations compared to the symmetric case. Analogously to the symmetric case, substantial changes in the gain spectrum for mode  $A_-$  correspond to energy transfer to mode  $A_+$  (not shown here). We have presented the impact of the input pump phase and power fluctuations in the PI operational regime. It is worth mentioning that in the phase-sensitive scenario (where idler waves are present at the input too), we find

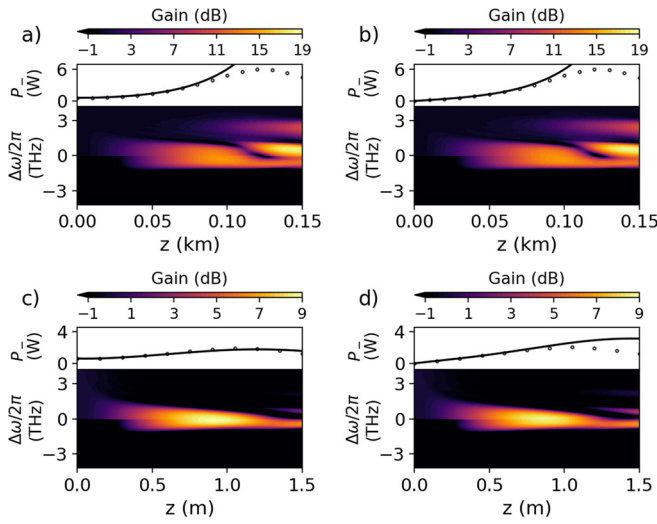


**FIG. 3.** PI gain for  $A_-$ : equivalence of amplitude and phase fluctuation effects. Map of parametric gain from numerical simulations vs  $z$  and frequency. Amplification in lossless coupled-core fibers: (a) ( $P_d = 600$  mW,  $\phi_d = 0$ ); (b) ( $P_d = 0$ ,  $\phi_d = 100$  mRad). Amplification in lossy coupled waveguides: (c) ( $P_d = 600$  mW,  $\phi_d = 0$ ); (d) ( $P_d = 0$ ,  $\phi_d = 100$  mRad). Evolution of  $P_-$  calculated analytically (solid) and numerically (dots) are shown as a reference. Other parameters used in (a) and (b) are:  $\beta_2 = -0.5$  ps<sup>2</sup> km<sup>-1</sup>,  $\gamma = 10$  W<sup>-1</sup> km<sup>-1</sup>,  $P_p = 6$  W,  $\alpha = 0$  km<sup>-1</sup>,  $C_0 = 15$  km<sup>-1</sup>,  $C_1 = -3$  ps km<sup>-1</sup>, and  $C_2 = 1$  ps<sup>2</sup> km<sup>-1</sup>; parameters used in (c) and (d) are:  $\beta_2 = -0.05$  ps<sup>2</sup> m<sup>-1</sup>,  $\gamma = 1.2$  W<sup>-1</sup> m<sup>-1</sup>,  $P_p = 6$  W,  $C_0 = 1.8$  m<sup>-1</sup>,  $C_1 = -0.3$  ps m<sup>-1</sup>,  $C_2 = 0.1$  ps<sup>2</sup> m<sup>-1</sup>, and  $\alpha = 0.69$  m<sup>-1</sup> corresponding to 3 dB m<sup>-1</sup>.

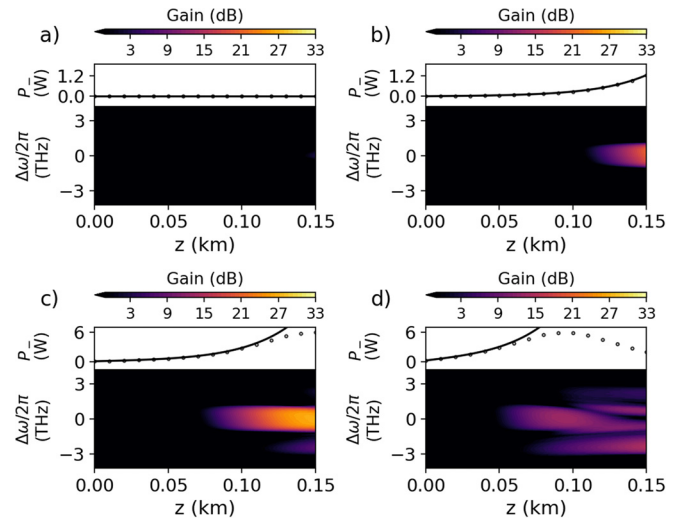


**FIG. 5.** Symmetrically pumped lossless PI gain for  $A_-$ . Map of parametric gain from numerical simulations vs  $z$  and frequency. (a) No fluctuations ( $P_d = 0$ ,  $\phi_d = 0$ ); (b)  $P_d = 4$  mW and  $\phi_d = 4$  mRad; (c)  $P_d = 40$  mW and  $\phi_d = 40$  mRad; and (d)  $P_d = 200$  mW and  $\phi_d = 200$  mRad. Evolution of  $P_-$  calculated analytically (solid) and numerically (dots) are shown as a reference. Remaining parameters used are the same as in Figs. 3(a) and 3(b).

results that are analogous, and we do not report here for the sake of brevity. A similar scenario occurs as well for a PI amplifier where the input signals are located in supermode  $A_+$  instead that in  $A_-$ .

Achieving two almost identical optical paths for the waves injected into the coupled-nonlinear-waveguide amplifier may result in

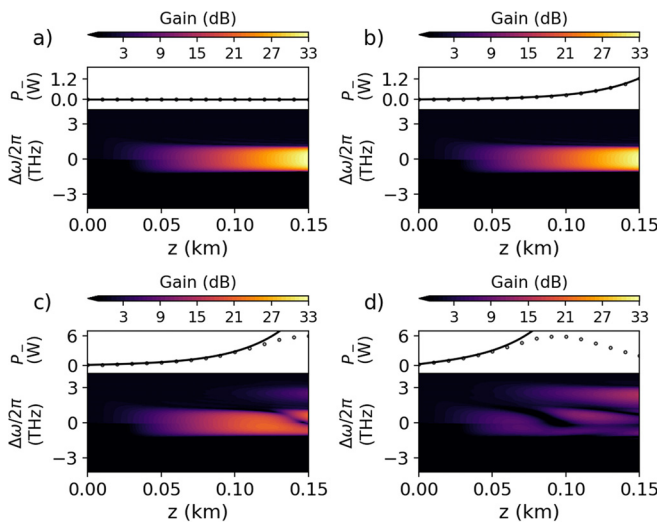


**FIG. 4.** Symmetrically pumped lossless PI gain for  $A_+$ . Maps of parametric gain from numerical simulations vs  $z$  and frequency. (a) No fluctuations ( $P_d = 0$ ,  $\phi_d = 0$ ); (b)  $P_d = 4$  mW and  $\phi_d = 4$  mRad; (c)  $P_d = 40$  mW and  $\phi_d = 40$  mRad; and (d)  $P_d = 200$  mW and  $\phi_d = 200$  mRad. Evolution of  $P_-$  calculated analytically (solid) and numerically (dots) are shown as a reference. Remaining parameters used are the same as in Figs. 3(a) and 3(b).

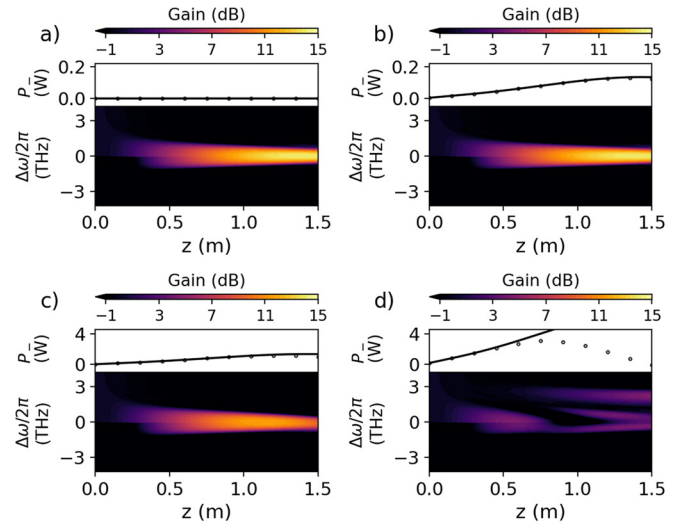


**FIG. 6.** Symmetrically pumped lossy PI gain for  $A_+$ . Maps of parametric gain calculated numerically vs  $z$  and frequency. (a) No fluctuations ( $P_d = 0$ ,  $\phi_d = 0$ ); (b)  $P_d = 4$  mW and  $\phi_d = 4$  mRad; (c)  $P_d = 40$  mW and  $\phi_d = 40$  mRad; and (d)  $P_d = 200$  mW and  $\phi_d = 200$  mRad. Evolution of  $P_-$  calculated analytically (solid) and numerically (dots) are shown as a reference. Remaining parameters used are the same as in Figs. 3(c) and 3(d).

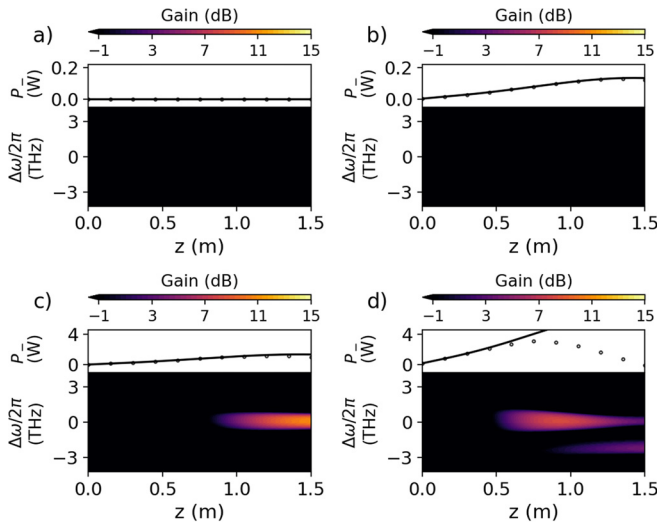


**FIG. 7.** Symmetrically pumped lossy PI gain for  $A_+$ . Map of parametric gain with numerical simulation vs  $z$  and frequency. (a) No fluctuations ( $P_d = 0, \phi_d = 0$ ); (b)  $P_d = 4$  mW and  $\phi_d = 4$  mRad; (c)  $P_d = 40$  mW and  $\phi_d = 40$  mRad; and (d)  $P_d = 200$  mW and  $\phi_d = 200$  mRad. Evolution of  $P_-$  calculated analytically (solid) and numerically (dots) are shown as a reference. Remaining parameters used are the same as in Figs. 3(c) and 3(d).

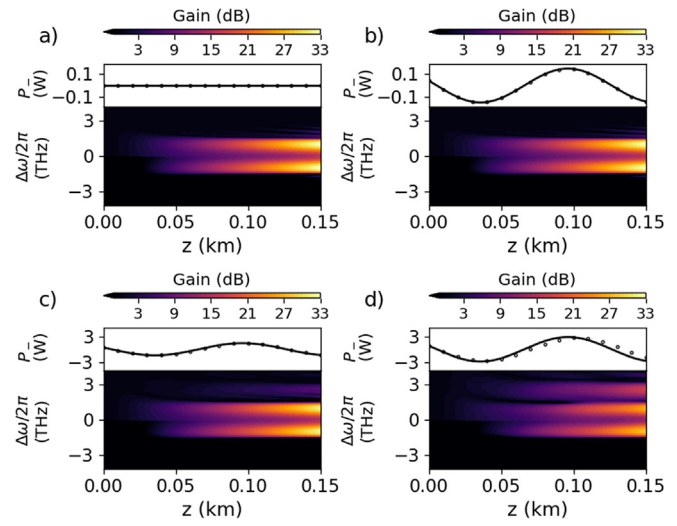


**FIG. 9.** Antisymmetrically pumped lossless PI gain for  $A_-$ . Maps of parametric gain from numerical simulations vs  $z$  and frequency. (a) No fluctuations ( $P_d = 0, \phi_d = 0$ ); (b)  $P_d = 40$  mW and  $\phi_d = 40$  mRad; (c)  $P_d = 400$  mW and  $\phi_d = 400$  mRad; and (d)  $P_d = 800$  mW and  $\phi_d = 800$  mRad. Evolution of  $P_-$  calculated analytically (solid) and numerically (dots) are shown as a reference. Remaining parameters used are the same as in Figs. 3(a) and 3(b).

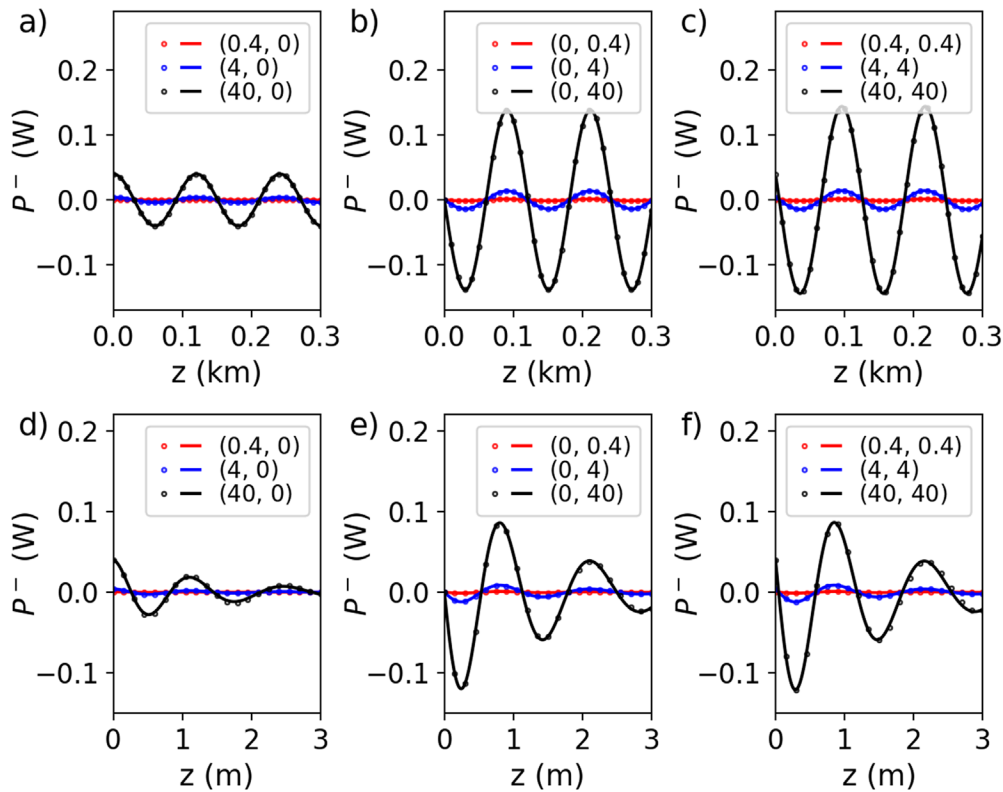


**FIG. 8.** Evolution of pump power difference for the antisymmetric case. (a)–(c) Evolution of  $P_-$  without losses calculated analytically (solid) and in numerical simulations (dots) for different values of  $P_d$  and  $\phi_d$  shown in the legends, where  $(x, y)$  represents  $P_d = x$  mW and  $\phi_d = y$  mRad. Parameters used are like Fig. 2(a). (d)–(f) Evolution of  $P_-$  with losses calculated analytically (solid) and in numerical simulations (dots). Parameters used are like Fig. 2(d).

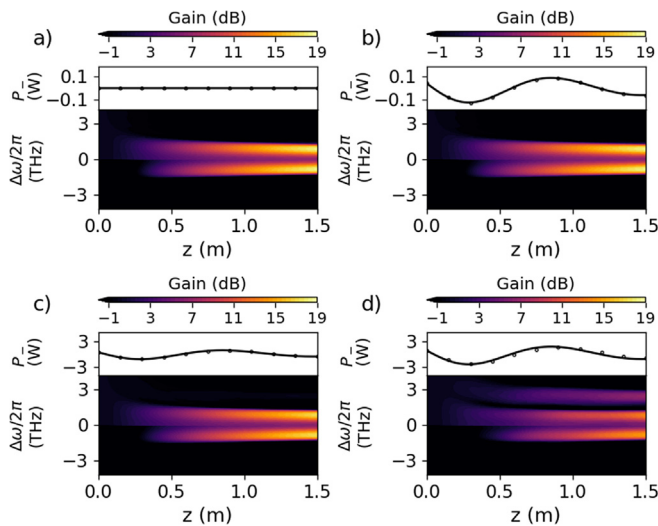


**FIG. 10.** Antisymmetrically pumped lossy PI gain for  $A_{-}$ . Maps of parametric gain from numerical simulations vs  $z$  and frequency. (a) No fluctuations ( $P_d = 0$ ,  $\phi_d = 0$ ); (b)  $P_d = 40$  mW and  $\phi_d = 40$  mRad; (c)  $P_d = 400$  mW and  $\phi_d = 400$  mRad; and (d)  $P_d = 800$  mW and  $\phi_d = 800$  mRad. Evolution of  $P_{-}$  calculated analytically (solid) and numerically (dots) are shown as a reference. Remaining parameters used are the same as in Figs. 3(c) and 3(d).

alignment issues that require special equipment for precise compensation. However, existing commercial phase-meters<sup>38</sup> enable phase control up to the order of  $6 \mu\text{rad}$ . This makes our parameters choice, regarding the gain spectrum degradation caused by large relative phase difference illustrated in the previous figures, a very pessimistic scenario. A very pessimistic scenario has been indeed considered for the cases of gain degradation caused by large values of input power differences too. An analysis based on current 50/50% couplers commercially available,<sup>39</sup> which have a coupling ratio tolerance of  $\pm 5\%$ , would predict relative differences of the order of  $\pm 50$  mW for a 1 W pump in the worst-case scenario. However, it is very important to stress that since the resolution of typical power meters is of the order of sub  $\mu\text{W}$ , it is possible to correct this imbalance, as it is not a fundamental one, without sophisticated technology, for instance, by using variable optical attenuators in each output port of the 50/50% couplers. Hence, it is likely feasible to achieve the performance of Figs. 4, 6(a), and 6(b) with minimum engineering effort and a negligible impact on the noise figure.

In conclusion, we have provided the analytical theory of pump waves stability for an equally pumped dual-waveguide parametric amplifier under the influence of relative input power and phase fluctuations. Our analytical theory predicts the evolution of pump power difference along the waveguides, and it is in good agreement with numerical simulations for realistic parameters. We have, furthermore, shown numerically how pump waves instability caused by power and phase fluctuations translates into amplifier gain spectrum changes, which occur for the magnitude of the input perturbations much larger than what can be realistically controlled in experiments. The results presented in this work hint at the resilience of equally pumped coupled dual-waveguide parametric amplifiers against pump fluctuations and can help the design of photonic technologies relying on this amplification scheme.

A.M.P. acknowledges support from the Royal Academy of Engineering through the Research Fellowship Scheme.

## AUTHOR DECLARATIONS

### Conflict of Interest

The authors have no conflicts to disclose.

## Author Contributions

**Minji Shi:** Conceptualization (equal); Formal analysis (equal); Investigation (equal); Writing – original draft (equal). **Vitor Ribeiro:** Conceptualization (equal); Methodology (equal); Writing – original draft (equal). **Auro M. Perego:** Conceptualization (equal); Formal analysis (equal); Investigation (equal); Methodology (equal); Supervision (equal); Writing – original draft (equal); Writing – review & editing (equal).

## DATA AVAILABILITY

The data that support the findings of this study are available from the corresponding author upon reasonable request.

## REFERENCES

- R. Stolen and J. Bjorkholm, "Parametric amplification and frequency conversion in optical fibers," *IEEE J. Quantum Electron.* **18**, 1062–1072 (1982).
- M. E. Mahric, *Fiber Optical Parametric Amplifiers, Oscillators and Related Devices: Theory, Applications, and Related Devices* (Cambridge University Press, 2007).
- M. E. Mahric, N. Kagi, T.-K. Chiang, and L. G. Kazovsky, "Broadband fiber optical parametric amplifiers," *Opt. Lett.* **21**, 573–575 (1996).
- J. Hansryd, P. A. Andrekson, M. Westlund, J. Li, and P. O. Hedekvist, "Fiber-based optical parametric amplifiers and their applications," *IEEE J. Sel. Top. Quantum Electron.* **8**, 506–520 (2002).
- P. A. Andrekson and M. Karlsson, "Fiber-based phase-sensitive optical amplifiers and their applications," *Adv. Opt. Photonics* **12**, 367–428 (2020).
- S. Olsson, H. Eliasson, E. Astra, M. Karlsson, and P. A. Andrekson, "Long-haul optical transmission link using low-noise phase-sensitive amplifiers," *Nat. Commun.* **9**, 2513 (2018).
- M. F. C. Stephens, V. Gordienko, and N. J. Doran, "20 dB net-gain polarization-insensitive fiber optical parametric amplifier with >2 THz bandwidth," *Opt. Express* **25**, 10597–10609 (2017).
- V. Gordienko, M. F. C. Stephens, A. E. El-Taher, and N. J. Doran, "Ultra-flat wideband single-pump Raman-enhanced parametric amplification," *Opt. Express* **25**, 4810–4818 (2017).
- M. Islam and O. Boyraz, "Fiber parametric amplifiers for wavelength band conversion," *IEEE J. Sel. Top. Quantum Electron.* **8**, 527–537 (2002).
- X. Liu, R. Osgood, Y. Vlasov, and W. Green, "Mid-infrared optical parametric amplifier using silicon nanophotonic waveguides," *Nat. Photonics* **4**, 557–560 (2010).
- P. Zhao, Z. Ye, K. Vijayan, C. Naveau, J. Schröder, M. Karlsson, and P. A. Andrekson, "Waveguide tapering for improved parametric amplification in integrated nonlinear  $\text{Si}_3\text{N}_4$  waveguides," *Opt. Express* **28**, 23467–23477 (2020).
- Z. Ye, P. Zhao, K. Twayana, M. Karlsson, P. A. Andrekson, and V. Torres-Company, "Ultralow-loss meter-long dispersion-engineered silicon nitride waveguides," in *Conference on Lasers and Electro-Optics* (Optical Society of America, 2021).
- Z. Ye, P. Zhao, K. Twayana, M. Karlsson, V. Torres-Company, and P. A. Andrekson, "Overcoming the quantum limit of optical amplification in monolithic waveguides," *Sci. Adv.* **7**, eabi8150 (2021).
- P. Zhao, M. Karlsson, and P. A. Andrekson, "Low-noise integrated phase-sensitive waveguide parametric amplifiers," *J. Lightwave Technol.* **40**, 128–135 (2022).

- <sup>15</sup>P. Zhao, Z. Ye, M. Karlsson, V. Torres-Company, and P. A. Andrekson, "Low-noise phase-sensitive parametric amplifiers based on integrated silicon-nitride-waveguides for optical signal processing," *J. Lightwave Technol.* **40**, 1847–1854 (2022).
- <sup>16</sup>A. Mecozzi, "Parametric amplification and squeezed-light generation in a nonlinear directional coupler," *Opt. Lett.* **13**, 925–927 (1988).
- <sup>17</sup>S. Trillo, S. Wabnitz, G. I. Stegeman, and E. M. Wright, "Parametric amplification and modulational instabilities in dispersive nonlinear directional couplers with relaxing nonlinearity," *J. Opt. Soc. Am. B* **6**, 889–900 (1989).
- <sup>18</sup>J. Janszky, C. Sibilia, M. Bertolotti, P. Adam, and A. Petak, "Properties of a directional coupler with parametric amplification," *Quantum Semiclassical Opt.* **7**, 509–516 (1995).
- <sup>19</sup>R. S. Tasgal and B. A. Malomed, "Modulational instabilities in the dual-core nonlinear optical fiber," *Phys. Scr.* **60**, 418–422 (1999).
- <sup>20</sup>A. A. Nair, K. Porsezian, and M. Jayaraju, "Impact of higher order dispersion and nonlinearities on modulational instability in a dual-core optical fiber," *Eur. Phys. J. D* **72**, 6 (2018).
- <sup>21</sup>R. Ganapathy, B. A. Malomed, and K. Porsezian, "Modulational instability and generation of pulse trains in asymmetric dual-core nonlinear optical fibers," *Phys. Lett. A* **354**, 366–372 (2006).
- <sup>22</sup>J. H. Li, K. S. Chiang, and K. W. Chow, "Modulation instabilities in two-core optical fibers," *J. Opt. Soc. Am. B* **28**, 1693–1701 (2011).
- <sup>23</sup>J. H. Li, K. S. Chiang, B. A. Malomed, and K. W. Chow, "Modulation instabilities in birefringent two-core optical fibres," *J. Phys. B* **45**, 165404 (2012).
- <sup>24</sup>J. H. Li, T. T. Sun, Y. Q. Ma, Y. Chen, Z. L. Cao, F. L. Xian, D. Z. Wang, and W. Wang, "Modulation instabilities in nonlinear two-core optical fibers with fourth order dispersion," *Optik* **208**, 164134 (2020).
- <sup>25</sup>J. H. Li, T. T. Sun, Y. Q. Ma, Y. Y. Chen, Z. L. Cao, and F. L. Xian, "The effects of fourth-order dispersion on modulation instabilities in two-core optical fibers with asymmetric CW state," *Phys. Scr.* **95**, 115502 (2020).
- <sup>26</sup>K. Nithyanandan, R. V. J. Raja, and K. Porsezian, "Modulational instability in a twin-core fiber with the effect of saturable nonlinear response and coupling coefficient dispersion," *Phys. Rev. A* **87**, 043805 (2013).
- <sup>27</sup>A. Govindarajan, B. A. Malomed, A. Mahalingam, and A. Uthayakumar, "Modulational instability in linearly coupled asymmetric dual-core fibers," *Appl. Sci.* **7**, 645 (2017).
- <sup>28</sup>A. M. Rubenchik, E. V. Tkachenko, M. P. Fedoruk, and S. K. Turitsyn, "Power-controlled phase-matching and instability of CW propagation in multicore optical fibers with a central core," *Opt. Lett.* **38**, 4232–4235 (2013).
- <sup>29</sup>J. H. Li, K. S. Chiang, and C. R. Li, "Modulation instability in collinear three-core optical fibers," *J. Opt. Soc. Am. B* **34**, 2467–2477 (2017).
- <sup>30</sup>V. Ribeiro, M. Karlsson, and P. Andrekson, "Parametric amplification with a dual-core fiber," *Opt. Express* **25**, 6234–6243 (2017).
- <sup>31</sup>V. Ribeiro, A. Lorences-Riesgo, P. Andrekson, and M. Karlsson, "Noise in phase-(in)sensitive dual-core fiber parametric amplification," *Opt. Express* **26**, 4050–4059 (2018).
- <sup>32</sup>V. Ribeiro and A. M. Perego, "Parametric amplification in lossy nonlinear waveguides with spatially dependent coupling," *Opt. Express* **30**, 17614–17624 (2022).
- <sup>33</sup>V. Ribeiro and A. M. Perego, "Theory of parametric amplification in coupled lossy waveguides," in *Conference on Lasers and Electro-Optics* (Optical Society of America, 2022).
- <sup>34</sup>A. D. Szabó, V. Ribeiro, C. B. Gaur, A. A. I. Ali, A. Mussot, Y. Quiquempois, G. Bouwmans, and N. J. Doran, "Dual-polarization C+L-band wavelength conversion in a twin-core highly nonlinear fibre," in *OFC Virtual Conference*, 2021.
- <sup>35</sup>V. Ribeiro, A. D. Szabó, A. M. Rocha, C. B. Gaur, A. A. I. Ali, Y. Quiquempois, A. Mussot, G. Bouwmans, and N. Doran, "Parametric amplification and wavelength conversion in dual-core highly nonlinear fibers," *J. Lightwave Technol.* **40**, 6013 (2022).
- <sup>36</sup>M. Shi, V. Ribeiro, and A. M. Perego, "Parametric amplification in coupled nonlinear waveguides: the role of coupling dispersion," *Front. Photonics* (submitted) (2023).
- <sup>37</sup>M. Shi, V. Ribeiro, and A. M. Perego, "Parametric amplification based on intermodal four-wave mixing between different supermodes in coupled core fibers," *Opt. Express* **31**, 9760–9768 (2023).
- <sup>38</sup>Liquid Instruments, see <https://www.liquidinstruments.com> for "Moku:Pro's phasemeter," accessed 26 November 2022.
- <sup>39</sup>Thorlabs, see [https://www.thorlabs.com/newgrouppage9.cfm?objectgroup\\_id=9567](https://www.thorlabs.com/newgrouppage9.cfm?objectgroup_id=9567) for "1550 nm 1x2 single mode fused fiber optic couplers taps," accessed 26 November 2022.